

Article

Improving the Corrosion Resistance of Zn-Rich Epoxy Coating with Three-Dimensional Porous Graphene

Zhihong Qin ¹, Yinqiang Su ², Yang Bai ³, Hangqi Lu ², Tao Peng ², Huifeng Zhong ², Tao Chen ² and Xusheng Du ^{4,*} 

- ¹ The Fifth Engineering Co., Ltd., MBEC, Jiujiang 332001, China; qinzhihong1987@163.com
² Zhuhai Communication Group, Zhuhai 519000, China; laosi188@163.com (Y.S.); lhq34500233@163.com (H.L.); pengtao13709690425@163.com (T.P.); zhfmerry@163.com (H.Z.); ct18666940946@163.com (T.C.)
³ CCCC-SHB Fifth Engineering Co., Ltd, Xi'an 710119, China; baiyang20051987@163.com
⁴ Institute of Advanced Wear & Corrosion Resistant and Functional Materials, Jinan University, Guangzhou 510632, China
* Correspondence: xdusydn@email.jnu.edu.cn

Abstract: To improve the corrosion inhibition of zinc-rich epoxy (ZRE) composite coatings and shed light on the influence of the spatial structure of graphene fillers on the coatings' performance, three-dimensional graphene (3DG) and a conventional graphene sheet (G) were used to modify the ZRE composite paint, respectively. The effect of introducing the 2D G fillers on the anti-corrosion behavior of ZRE was studied comprehensively, and its optimal content was determined to be 0.5 wt%. Interestingly, it was found that, comparing with 2D graphene sheets, the corrosion resistance of the ZRE coating could be enhanced more significantly with incorporating even less 3DG. With introducing only 0.1 wt% 3DG, the corrosion current intensity of the resulting 3DG/ZRE coating was reduced to be about 1/10 that of the G/ZRE coating with the same graphene content and 27% of that of the optimized G/ZRE. The corrosion products of the coating were analyzed with the XRD technique. The results indicated that, in contrast to neat ZRE coating, $Zn_5(CO_3)_2(OH)_6$ was absent from the corroded 3DG/ZRE coating, confirming its improved long-term anti-corrosion performance. The porous interconnected framework and high crystallinity of 3DG could contribute to not only its facilely mixing with epoxy resin, but also its effective incorporation into the conductive network of zinc micro-flakes, thus enhancing the corrosion resistance of its ZRE coating at a lower content. The innovative technology to improve the anti-corrosion performance of the ZRE coatings via using the 3D graphene fillers should be capable to be extended to other 2D fillers, such as MXenes.



Citation: Qin, Z.; Su, Y.; Bai, Y.; Lu, H.; Peng, T.; Zhong, H.; Chen, T.; Du, X. Improving the Corrosion Resistance of Zn-Rich Epoxy Coating with Three-Dimensional Porous Graphene. *Polymers* **2023**, *15*, 4302. <https://doi.org/10.3390/polym15214302>

Academic Editor: Qing Wu

Received: 30 August 2023

Revised: 11 October 2023

Accepted: 25 October 2023

Published: 1 November 2023



Copyright: © 2023 by the authors. Licensee MDPI, Basel, Switzerland. This article is an open access article distributed under the terms and conditions of the Creative Commons Attribution (CC BY) license (<https://creativecommons.org/licenses/by/4.0/>).

1. Introduction

Recently, two-dimensional (2D) multi-functional materials, including graphene, graphitic carbon nitride, and MXene, have aroused extensive research interest all over the world, and a large amount of work on their facile fabrication and applications in many fields [1–4]. Carbon materials, such as the well-known graphene and amorphous carbon coatings, have been applied for the surface protection of various metals [5–7]. Due to their unique characters, including an excellent barrier property, high chemical stability, and lubricating behavior, these carbon materials as coatings exhibit a high anti-corrosive and anti-scratch performance. Another method to exploit fully their functional property in the surface protection of metallic substrate is achieved by incorporating them into polymer composite coatings [8–15]. It is suggested that graphene sheets incorporated into a zinc-rich epoxy (ZRE) composite coating will make the best use of the cathodic protection of zinc powders in the coatings through facilitating the construction of a conductive network between zinc particles. Up to now, many types of carbon materials have been investigated for

this aim, including one-dimensional (1D) carbon fibers [16] or nanotubes [17], and 2D graphenes [18,19].

Due to their high aspect ratio and 2D structure, graphene sheets are ready to aggregate in the polymer matrix, resulting in a great challenge to prepare their composite with a high performance. To alleviate this, graphene derivatives, including graphene oxide or fluorinated reduced graphene oxide, have been developed and used to prepare the composites [20–23]. However, the derivatives generally have the deteriorated conductivity due to their decreased crystallinity or even being in an amorphous state.

Graphene foam has been developed in recent years. The most common method to prepare the foam is the so-called chemical vapor deposition method. With this method, the porous structure of graphene is controlled by the metal catalytic foam templates, and the thickness of the graphene foam strut-wall can be controlled to be within nanometers. Due to their unique porous 3D structures, their polymer composites with various advanced properties [24–26], including high wear resistance and electrical or thermal conductivity, have been developed and investigated as multi-functional composites [25,26]. However, little information on its application in anti-corrosive zinc-rich coating is available so far.

In this work, the influence of the spatial structure of high-crystalline graphene fillers on the corrosion resistance of ZRE coatings was studied. Besides conventional 2D graphene sheets, 3DG with a porous structure and interconnected graphene framework has been applied to modify the ZRE paint. Both the morphology and physical chemical properties of the as-prepared 3DG will be characterized. To avoid the influence of the crystalline structure of graphene on the anti-corrosive behavior of the modified ZRE coating, 3DG with a similar crystalline structure to graphene sheets has been used in this study. The anti-corrosion behaviors of the ZRE modified with different graphenes in the artificial simulated seawater (3.5 wt% NaCl solution) will be studied by the potentiodynamic polarization test and electrochemical impedance spectroscopy, as well as the long-term immersion test.

2. Materials and Methods

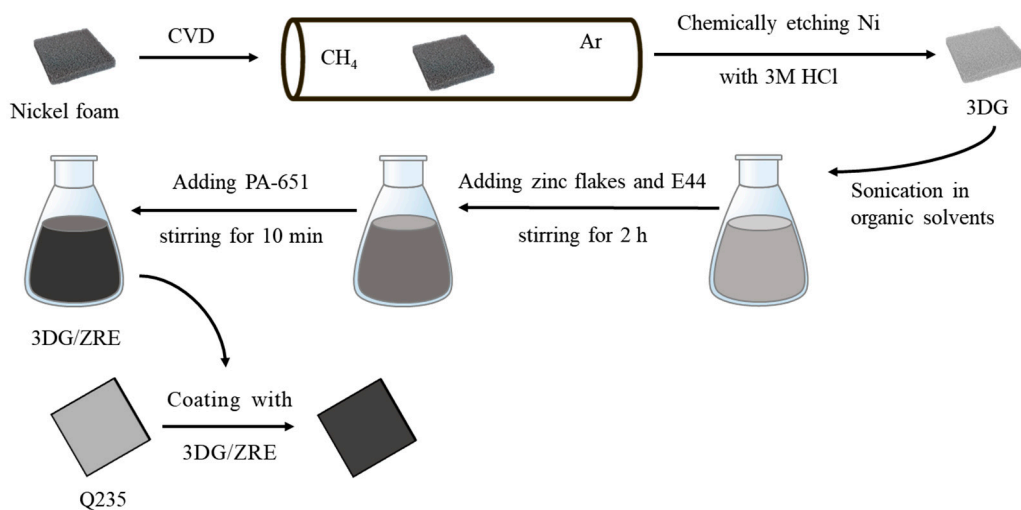
2.1. Materials

Commercial graphene sheets (G, lateral size of 10~50 μm and thickness of 3–8 nm) were purchased from Suzhou Tanfeng Technology Co. Ltd. (Suzhou, China). Epoxy (E-44) was provided by Xiya Reagent Co. (Shangdong, China). Xylene, n-butanol, and polyamide 651 were all chemically pure and purchased from McLean Group. (McLean, VA, USA) Commercial zinc flakes with a lateral size of 5–15 μm were ordered from Xiamen Empire New Material Technology Co. Ltd. (Xiamen, China) and a Q235 steel plates with a size of 30 mm \times 40 mm were provided by Fuquan Metal Co. Ltd. (Quanzhou, China).

2.2. Preparation of Composite Paint and Coating Samples

The whole process was illustrated as Scheme 1. As depicted in previous work [25], graphene foam was produced by the template-directed chemical vapor deposition (CVD) method following the removal of Ni foam. It was then used to prepare 3DG/ZRE paint. The epoxy composite paint comprised two parts, i.e., the component A (epoxy resin and Zn powder) and component B (polyamine curing agent, PA-651). For the fabrication of the modified paint, common graphene or graphene foam was firstly dispersed into epoxy resin diluent ultrasonically. After adding E-44 and Zn powder, the dispersion was magnetically stirred for 2 h. The paint was fabricated finally by mixing it with component B. In the paint composite system, organic solvent (xylene: n-butanol = 7:3) was used as the epoxy diluent and its mass fraction in the paint was 20 wt%. The mass fraction of E-44, zinc powder, and PA-651 is 30 wt%, 35 wt%, and 15 wt%, respectively. Depending on the fraction of graphene (0.1 wt%, 0.3 wt%, 0.5 wt%, and 0.7 wt%) or 3 DG (0.1 wt%), the resulted coatings were labeled as ‘the fraction G/ZRE’ or ‘0.1 wt% 3DG/ZRE’, respectively. Prior to being coated with the ZRE paint, Q235 carbon steel plates were sandblasted and washed with acetone. The paint was applied to the surface of the sandblasted Q235 plates by a rod applicator and

cured in an oven at 60 °C for 24 h. Moreover, neat ZRE coating was prepared using the same method in the absence of any graphene filler.



Scheme 1. Schematic diagram of the process for the preparation of 3DG/ZRE composite and its coating on the Q235 steel plate.

2.3. Characterization Methods

The crystalline structures of the graphene samples were characterized with an X-ray diffraction analyzer (Rigaku Ultima IV, Nagano, Japan). The carbon structure of 3DG was analyzed with a Raman spectrometer (Invia Renishaw Raman, Vignate Gieres, France). The morphology of the carbon sample was observed with a scanning electron microscope (SEM; Hitachi S4800, Tokyo, Japan). An optical microscope (DM3000) was also utilized to observe the morphology of graphene fillers in epoxy resin.

The corrosion measurements of the ZRE coatings were measured on a CHI 760e electrochemical analyzer. A three-electrode half-cell system was constructed with a saturated calomel electrode (SCE) as the reference electrode, platinum plate as the auxiliary electrode, and ZRE coated Q235 plates as the working electrode. First of all, an open circuit potential test (OCP) of the sample was performed to ensure it reached a relative steady state. The potentiodynamic polarization test was carried out at a scan rate of 10 mV s⁻¹ and its potential range was set to be ±250 mV around the OCP. Three potentiodynamic polarization tests were carried out for both neat ZRE and 3DG/ZRE samples and the typical ones are reported in the work. The electrochemical impedance spectroscopy (EIS) tests were performed in a frequency range of 10 kHz~0.1 Hz at room temperature. The simulated seawater (3.5 wt% NaCl solution) was used as the corrosive electrolyte.

3. Results and Discussion

3.1. Structure Characterization of G and 3DG

Different from the common 2D morphology of normal graphenes (Figure 1a), 3DG is a porous graphene monolith, which is composed of an interconnected hollow graphene framework (highlighted by red arrows in Figure 1b). Such a rich porous structure results from the metal framework template, which acts as the catalytic substrate for continuously growing graphene. Similar to the 3D porous amorphous carbon fabricated with the flame coating of Ni foam [27], grain boundaries replicating Ni substrate could be clearly observed in the high-magnification SEM image of the 3DG strut surface (see the inset in Figure 1b). Evidently, the graphene surface of 3DG is totally different from the conventional 2D graphene products, whose smooth surface is clearly shown as Figure 1a. These grain boundaries of 3DG may be helpful to improve their interface with epoxy matrix. Due to the porous framework and interconnected hollow strut structure of 3DG and the well-known

capillary action, organic liquids could mix well with it, as such liquids could infiltrate easily into the porous 3DG.

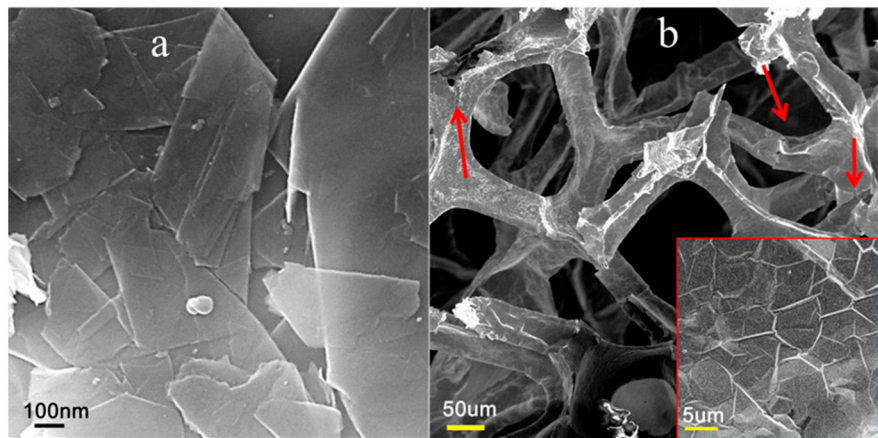


Figure 1. SEM images of graphene sheets (**a**) and 3DG (**b**).

Under the magnetic stirring in epoxy resin, the graphene framework monolith infiltrated with epoxy resin will be *in situ* broken into small fragment particles, whose morphology will have 3D irregular characteristics with a size larger than that of the conventional 2D graphene sheets [24]. As shown in Figure 2a, 3DG fragments are dispersed in the epoxy resin after the mixing process and they are much larger than those common graphene sheets in Figure 2b. It is noted that some struts could be observed occasionally in Figure 2a. The SEM image of the 3DG/ZRE composite confirms the presence of the large size of 3DG fragments, which are highlighted by the yellow arrows in Figure 2c. Evidently, they are surrounded by small Zn flakes in the composites. In contrast, it can be seen that small graphene sheets (highlighted by blue arrows in Figure 2d) appear together with Zn flakes, making it hard to define them from each other sometimes in the G/ZRE composites due to their similar 2D morphology. The large size and unique spatial structure of the 3DG fragments are expected to not only alleviate the re-stack of graphene sheets in the polymer matrix, but also favor the formation of the electric conductive path between Zn micro-flakes in the ZRE coatings, which helps to fully exert their cathodic protection function.

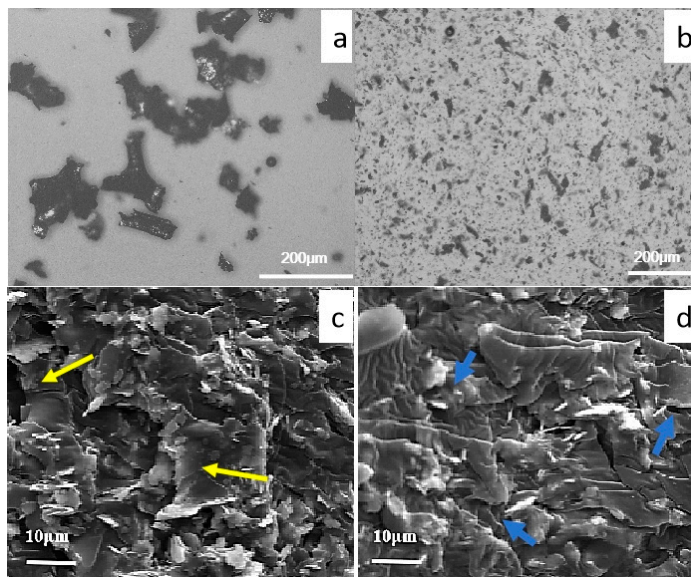


Figure 2. Optical image of the carbon fillers dispersed in epoxy resin: (**a**) 3DG and (**b**) graphene sheets; SEM images of the ZRE coatings: (**c**) 3DG/ZRE and (**d**) G/ZRE.

Similar to the research on the graphene deposited on catalytic metal substrates in the literature [6,28], two strong peaks for the G band at 1576.7 cm^{-1} and the 2D band at 2700 cm^{-1} , together with a very weak peak for the D band around 1357 cm^{-1} , could be observed in the Raman spectrum of 3DG (Figure 3). As the D band refers to the disorder carbon structure, and the relative intensities I_D/I_G could be used to evaluate the defect degree of carbonaceous structure, the Raman spectrum of 3DG confirms its high crystalline structure. Moreover, the intensity ratio (I_{2D}/I_G) of 3DG is 0.66, which is much less than 1, implying its multi-layered structure [6,7,29].

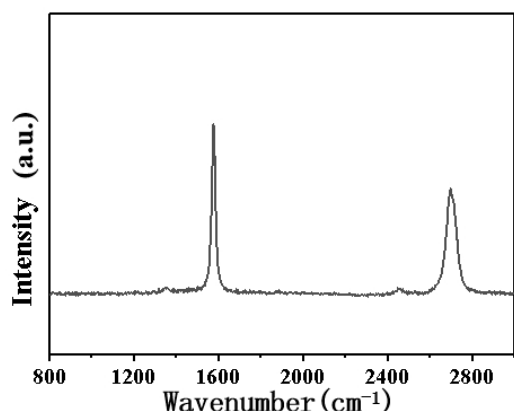


Figure 3. Raman spectrum of 3DG.

Figure 4a shows the XRD patterns of both 3DG and normal 2D graphene (G). It can be seen that 3DG displays a strong peak around 26° , which belongs to the (002) of graphite. Its pattern is similar to that of common 2D graphene sheets, suggesting that both samples have a high crystalline structure. Moreover, based on the strong peak in XRD patterns in Figure 4a, the average crystallite size of 3DG is calculated to be 40.5 nm, which is much larger than that of graphene sheets (19.8 nm). Furthermore, 3DG displays a much smaller lattice strain (0.000856) and dislocation density (0.000609) than graphene sheets, whose counterpart value is 0.002550 and 0.001752, respectively. These results demonstrate the high-quality continuous graphene struts in 3DG, which favor their electrical linkage with zinc particles in the ZRE coating. In the graphene-modified ZRE coating, quite a few strong peaks appear around 40° (Figure 4b). They majorly originate from the large amount of Zn flakes in the coating. Due to the low content of graphene in the composite, the peak contributed from graphene (26°) is too weak to be defined. For 3DG/ZRE samples, its XRD pattern is almost the same as that of 0.5 wt% G/ZRE.

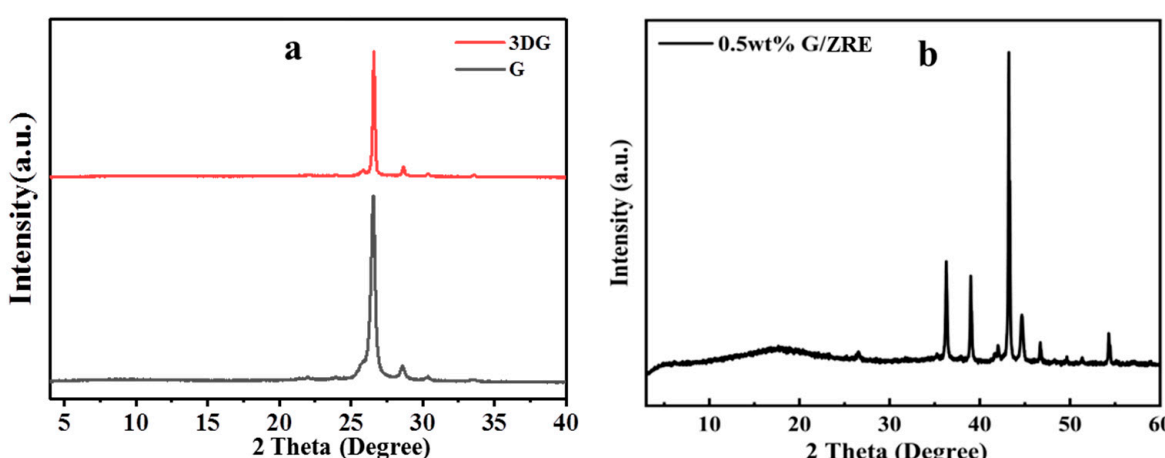


Figure 4. XRD patterns of (a) graphene sheets and 3DG, (b) 0.5 wt% G/ZRE.

3.2. Corrosion Inhibition of the Coatings

3.2.1. Corrosion Inhibition of Graphene Modified ZRE Coatings

The potentiodynamic polarization tests have been performed to characterize the corrosion inhibition behavior of various ZRE coatings. As shown in Figure 5, when incorporating G in the ZRE coating, the Tafel curves of all the samples move downwards, indicating the decreased corrosion current density (I_{corr}). Evidently, the lowest curve of the G/ZRE coating is the one containing 0.5 wt.% G. Based on Figure 5, the I_{corr} , corrosion potential (E_{corr}), and polarization resistance (R_{po}) of the coatings modified with different G content are obtained, and they are listed in Table 1. The I_{corr} value of neat ZRE is comparable with the other ZRE coating [30]. It can be found that, with the modification by only 0.1 wt.% G, the corrosion inhibition performance of the coating is already enhanced greatly, as its I_{corr} becomes to be only 1/3 that of neat ZRE coating. With the G content increasing from 0.1 to 0.5 wt.%, the I_{corr} of its ZRE coating decreases correspondingly (Figure 5). At 0.5 wt.% G, the I_{corr} of its ZRE coating is the lowest ($7.14 \times 10^{-7} \text{ A cm}^{-2}$), which means a ~10-fold improvement in the corrosion resistance, comparing with that of neat ZRE ($6.1 \times 10^{-6} \text{ A cm}^{-2}$). However, when further increasing the G content to 0.7 wt.%, the I_{corr} of its ZRE coating increases (Table 1). The increased I_{corr} of the coating could be due to the aggregation of G at high content, which deteriorates the barrier property of the coating. Additionally, the 0.5 wt.% G/ZRE coating displays the largest R_{po} among all the G/ZRE samples. As a result, 0.5 wt.% is determined to be the optimal G content for modifying ZRE coating.

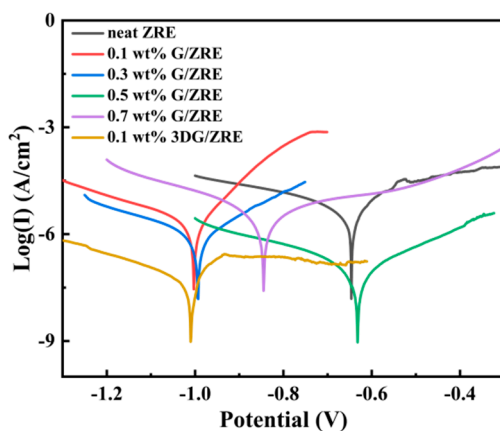


Figure 5. Tafel curves of different ZRE-coated Q235 steel plates in simulated seawater.

Table 1. I_{corr} , E_{corr} , and R_{po} of different ZRE-coated Q235 steel plates in simulated seawater.

ZRE Samples	I_{corr} ($\text{A} \cdot \text{cm}^{-2}$)	E_{corr} (V)	R_{po} ($\Omega \cdot \text{cm}^2$)
neat ZRE	6.11×10^{-6}	-0.646	5.67×10^3
0.1 wt% G/ZRE	1.95×10^{-6}	-1.002	1.31×10^4
0.3 wt% G/ZRE	1.15×10^{-6}	-0.993	3.21×10^4
0.5 wt% G/ZRE	7.14×10^{-7}	-0.631	3.65×10^5
0.7 wt% G/ZRE	3.36×10^{-6}	-0.844	1.27×10^4
0.1 wt% 3DG/ZRE	1.90×10^{-7}	-1.010	5.04×10^5

3.2.2. Corrosion Resistance of 3DG Modified ZRE Coatings

For the first time, it was revealed that the anti-corrosion performance of ZRE coating was capable to be further enhanced by replacing common G with 3DG, which exhibits a similar high crystalline structure. Due to its 3D porous structure, only 0.1 wt% 3DG is needed to modify the ZRE coating. As shown in Figure 5, its Tafel test curve moved downwards a little bit, along with the decreased I_{corr} , relative to that of 0.5 wt% G/ZRE. Its I_{corr} was $1.9 \times 10^{-7} \text{ A cm}^{-2}$, which was reduced to be nearly one quarter that of 0.5 wt%

G/ZRE, as shown in Table 1. Its R_{po} also became much larger than that of 0.5 wt% G/ZRE. These results demonstrate the greatly positive effect of 3DG in promoting the corrosion resistance of the ZRE coating.

The long-term corrosion resistance behavior of the ZRE coating was evaluated by the immersion test. It was suggested that the open circuit voltage (OCP) of the ZRE coating could be used as a factor to evaluate their protection performance [31]. Figure 6a shows the variation of OCP values of the three ZRE through the 300 h immersion test. Initially, the values of all the coating samples are far lower than -0.6 V. All the OCP values of the ZRE coatings increase quickly within the first 2-day immersion. This could be due to the oxidation of zinc particles and the formation of the corresponding compounds as the corrosive species continuously penetrate into the ZRE coating. Theoretically, the cathodic protection function of the coating will be reduced by the generation of the less conductive corrosion products due to the destruction of electrical linkage between zinc particles. Comparing with neat ZRE and G/ZRE, it takes much more time (~ 170 h) for 3DG/ZRE to reach a relative stable value, which means more zinc particles are involved in the sacrificial anode-based cathodic protection process. These results confirm the pronounced effect of 3DG fillers on maximizing the cathodic protection of ZRE coating.

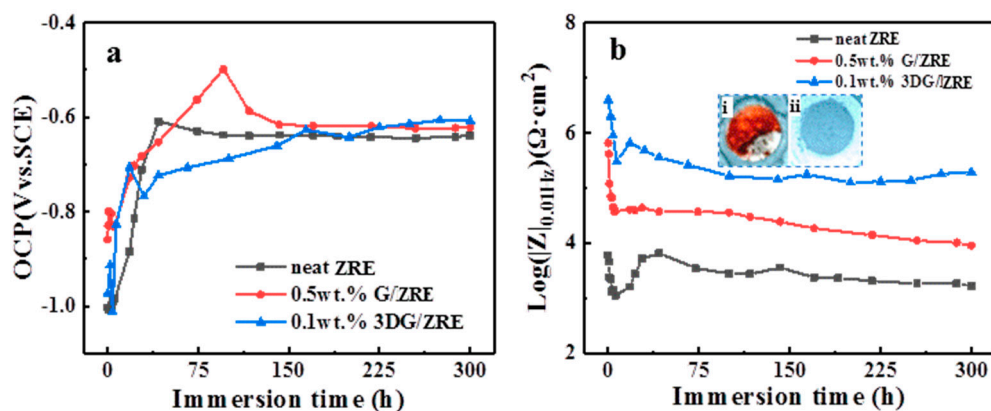


Figure 6. The dependence of (a) OCP and (b) $|Z|_{0.01\text{Hz}}$ on the immersion time for neat ZRE-, G/ZRE-, and 3DG/ZRE-coated Q235 steel plates.

The dependence of $|Z|_{0.01\text{Hz}}$ of the ZRE coatings on the time is shown in Figure 6b, where the $|Z|_{0.01\text{Hz}}$ of all the coatings decreased quickly with the immersion time initially. Obviously, 0.5 wt% G/ZRE exhibited a larger $|Z|_{0.01\text{Hz}}$ than neat ZRE during the whole immersion test, confirming the positive effect of incorporating G on promoting the corrosion inhibition of ZRE coating. Additionally, the curve of 0.1 wt% 3DG/ZRE is always higher than that of 0.5 wt% G/ZRE all through the immersion process, demonstrating the superior effect of 3DG over the 2D graphene on enhancing the corrosion resistance of ZRE coating. The digital image of the exposed circle area of neat ZRE after the immersion test indicates that its major part is brown, together with some white areas (the inset photo i in Figure 6b). The brown area is caused by the Fe^{3+} -containing corrosion product of steel substrate and the white area should be attributed to the zinc-containing corrosion products, which confirm the severe failure of the coating. In contrast, such a phenomenon is totally absent in the 0.1 wt% 3DG/ZRE sample (the inset photo ii in Figure 6b). Furthermore, after 300 h immersion in the simulated seawater, the Tafel curve of the 0.1 wt% 3DG/ZRE exhibits the smallest I_{corr} among all the three ZRE samples, as shown in Figure 7 and Table 2. Its I_{corr} ($5.2 \times 10^{-7} \text{ A cm}^{-2}$) is nearly 1/10 that of 0.5 wt% G/ZRE ($4.02 \times 10^{-6} \text{ A cm}^{-2}$) (Table 2). Additionally, its R_{po} is remarkably larger than that of 0.5 wt% G/ZRE as well. All of these experimental results confirm the significantly improved corrosion resistance of 0.1 wt% 3DG/ZRE.

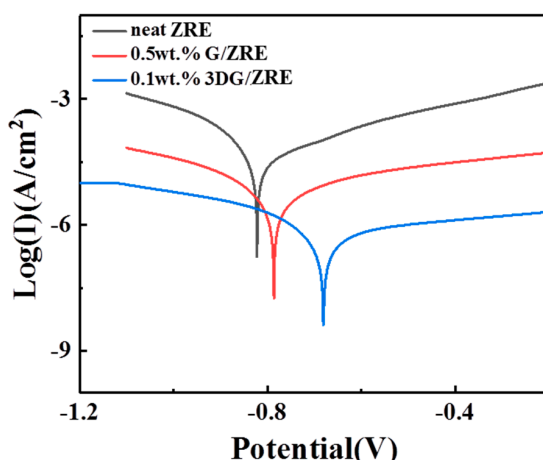


Figure 7. Tafel curve of neat ZRE-, G/ZRE-, and 3DG/ZRE-coated Q235 steel plates after 300 h immersion in simulated seawater.

Table 2. The I_{corr} , E_{corr} , and R_{po} of neat ZRE-, G/ZRE-, and 3DG/ZRE-coated Q235 steel plates after 300 h immersion in simulated seawater.

Samples Soaking for 300 h	I_{corr} ($A \cdot cm^{-2}$)	E_{corr} (V)	R_{po} ($\Omega \cdot cm^2$)
neat ZRE	4.87×10^{-5}	-0.824	7.76×10^2
0.5 wt% G/ZRE	4.02×10^{-6}	-0.786	9.89×10^3
0.1 wt% 3DG/ZRE	5.20×10^{-7}	-0.681	8.98×10^4

The Nyquist plots of the ZRE coatings after being soaked in simulated seawater are presented in Figure 8a. The equivalent circuit models used for the analysis of EIS data are illustrated in Figure 8b, where R_s represents the electrolyte resistance and R_p and CPE-1 represent the ZRE coating pore resistance and constant phase element of the ZRE capacitor, respectively, whereas R_{ct} and CPE-2 refer to the constant phase element and charge transfer resistance of double-layer capacitor [30,32]. The fitted data for the three ZRE coatings are listed in Table 3. R_{ct} could be used to evaluate a coating's corrosion resistance and a high R_{ct} value always meant a low-speed corrosion reaction. It can be found that the R_{ct} of 0.1 wt% 3DG/ZRE ($5.99 \times 10^5 \Omega \cdot cm^{-2}$) was ~46 times that of 0.5 wt% G/ZRE ($1.29 \times 10^4 \Omega \cdot cm^{-2}$), which agreed well with the aforementioned Tafel test results (Table 1). This implies the greatly decelerated corrosion of the ZRE coating with the modification of 3DG. Moreover, the larger R_p value generally meant a better physical barrier property of a coating [30]. The R_p of 0.1 wt% 3DG/ZRE ($3.59 \times 10^4 \Omega \cdot cm^{-2}$) was ~10 times that of 0.5 wt% G/ZRE ($3.53 \times 10^3 \Omega \cdot cm^{-2}$) (Table 3), indicating the significant effect of 3DG on improving the anti-corrosion property of the ZRE coating. Additionally, the smaller CPE-2 of 0.1 wt% 3DG/ZRE coincided this conclusion, as this capacitance was suggested to correspond to the barrier properties of the coatings at a high frequency [33]. The positive effect of 3DG should be related to its unique 3D structure, which facilitates its mixing with epoxy, hinders the permeation of the corrosives, and interconnects Zn particles, thus enhances the corrosion resistance of its ZRE coating.

Table 3. Eletrochemical parameters obtained from EIS data of different ZRE-coated Q235 steel.

ZRE Samples	CPE-1 ($S \cdot cm^{-2} \cdot s^n$)	$R_p (\Omega \cdot cm^2)$	CPE-2 ($S \cdot cm^{-2} \cdot s^n$)	$R_{ct} (\Omega \cdot cm^2)$	Model
neat ZRE	6.84×10^{-4}	-	-	8.37×10^3	A
0.5 wt% G/ZRE	7.19×10^{-7}	3.53×10^3	1.03×10^{-4}	1.29×10^4	B
0.1 wt% 3DG/ZRE	5.02×10^{-8}	3.59×10^4	1.23×10^{-5}	5.99×10^5	B

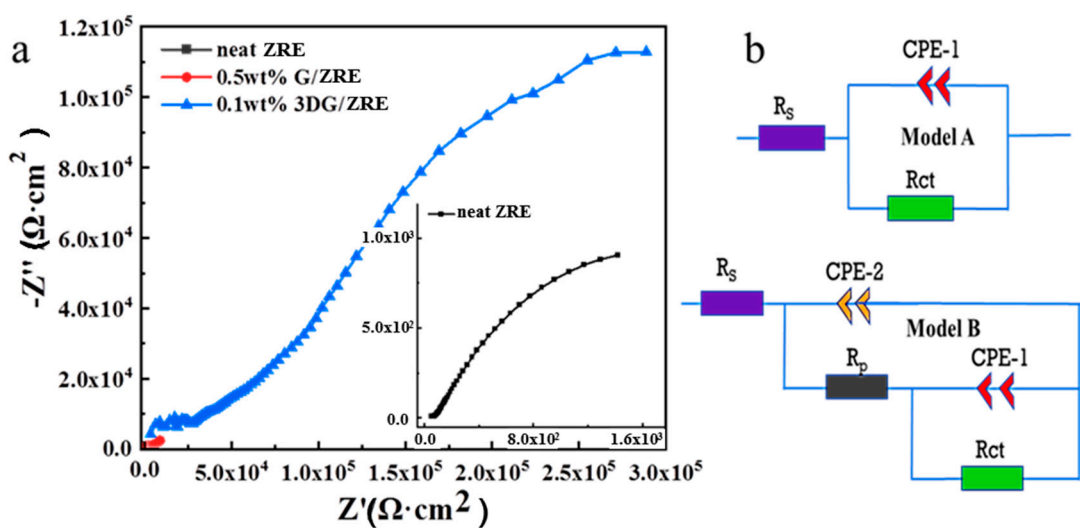
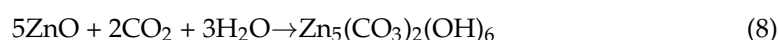
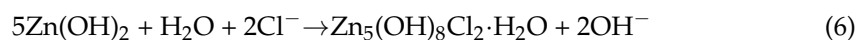
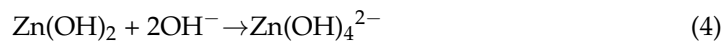


Figure 8. (a) Nyquist diagrams of neat ZRE-, G/ZRE-, and 3DG/ZRE-coated Q235 steel plates after 300 h immersion in the simulated seawater and (b) the equivalent circuit.

As suggested in the literature [34,35], the electrochemical reactions related to the zinc-containing products during the corrosion process of ZRE are given as the following Equations (1)–(9). Besides $\text{ZnO}/\text{Zn}(\text{OH})_2$ products (Equations (1)–(5)), the insoluble complexes, including Willemite (Equations (6)) and hydrozincite (Equations (7)–(9)), could be also formed under certain conditions (pH, the concentration of Cl^- and dissolved CO_2). After the continuous 300 h immersion test, the Q235 steel plates coated with either neat ZRE or 3DG/ZRE were taken out from the simulated seawater and their XRD patterns were taken to characterize the corrosion products. Consistent with the zinc corrosion products reported previously [36,37], many peaks in the XRD pattern of the soaked neat ZRE sample (Figure 9) could be attributed to ZnO , $\text{Zn}_5(\text{OH})_8\text{Cl}_2\text{H}_2\text{O}$, and $\text{Zn}_5(\text{CO}_3)_2(\text{OH})_6$, respectively. Interestingly, different from the presence of both complicated complex products on the soaked neat ZRE coating, no peak contributed from hydrozincite $\text{Zn}_5(\text{CO}_3)_2(\text{OH})_6$ could be found on the pattern of the 3DG/ZRE coating after the 300 h immersion test. This could be due to the excellent barrier property of 3DG particles to carbon dioxide, demonstrating its great contribution to the surface protection of the ZRE coating.



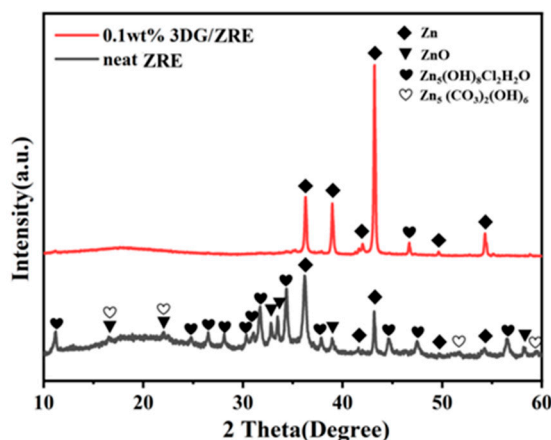


Figure 9. XRD patterns of neat ZRE- and 3DG/ZRE-coated Q235 steel plates after 300 h immersion in simulated seawater.

As shown in Figure 10d, after the immersion test, the corroded surface of the 3DG/ZRE coating became a little rougher than that before the test (Figure 10c) and small pores could be observed. These could be due to the oxidation of zinc particles in the coating and the formation of ZnO and Zn₅(OH)₈Cl₂H₂O, as mentioned above. In contrast, a more significant morphology change occurred for the neat ZRE-coated sample after the immersion test, as indicated in Figure 10a,b. Both the larger pores and the crack in Figure 10b confirm the seriously corroded neat ZRE-coated Q235 steel plate, which are inconsistent with the digital images shown in Figure 6 and the XRD analysis results mentioned above.

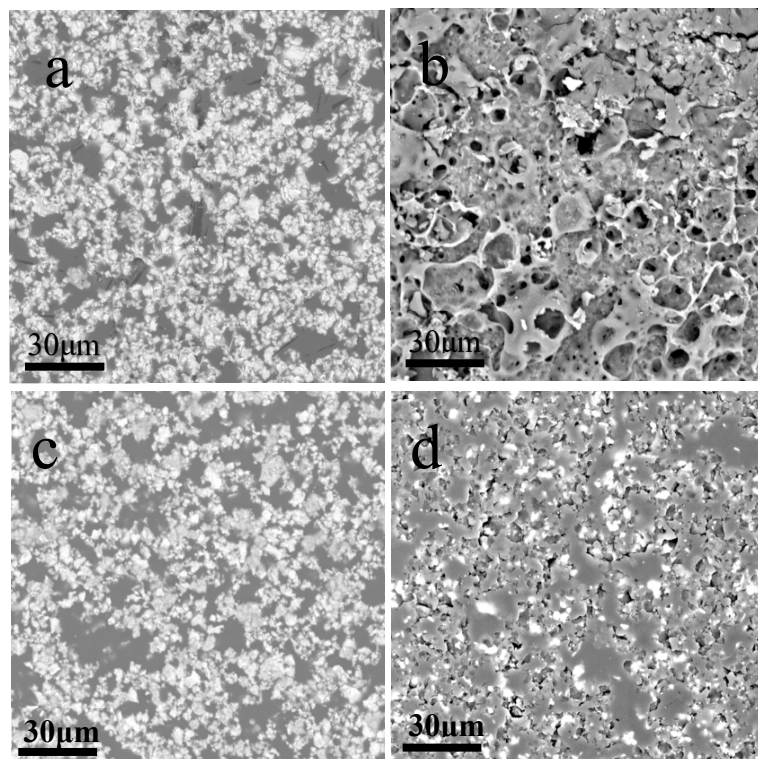


Figure 10. SEM images of ZRE-coated Q235 steel samples in simulated seawater: neat ZRE before (a) and after (d) 300 h immersion; 3DG/ZRE before (c) and after (d) 300 h immersion.

4. Conclusions

In this work, conventional 2D graphene sheets and 3DG fillers were used to modify the ZRE composite to improve the corrosion resistance of the ZRE coatings. These main conclusions are drawn:

- (1) The corrosion resistance of the ZRE coating could be improved by incorporating common 2D graphene, and the optimal G content is 0.5 wt%.
- (2) The corrosion resistance of the ZRE coating could be further enhanced significantly by incorporating only 0.1 wt% 3DG.
- (3) Long-term immersion tests confirmed the superior effect of 3DG on improving the surface protection performance of ZRE as well.

This work revealed, preliminarily, the significant effect of 3D graphene fillers on the surface protection performance of ZRE coating. However, to understand the spatial structure of graphene fillers on the properties of their ZRE coatings more comprehensively, further work needs to be done, such as the mathematical simulation of the contribution of 3DG to the cathodic protection process of ZRE coating.

Author Contributions: Conceptualization, Z.Q. and X.D.; methodology, Y.S., Y.B. and H.L.; validation, T.P. and T.C.; investigation, Z.Q., Y.S. and H.Z.; writing, Z.Q. and X.D.; funding acquisition, X.D. All authors have read and agreed to the published version of the manuscript.

Funding: This research received funding and support from Guangdong Province Science and Technology Plan (Project No. 2021A0505030041).

Institutional Review Board Statement: Not applicable.

Data Availability Statement: Experimental data from this study are available upon request.

Acknowledgments: We would like to acknowledge the support by the Department of Science and Technology of Guangdong Province of China.

Conflicts of Interest: Author Z.Q. and Y.B. were employed by the company the Fifth Engineering Co., Ltd. and CCCC-SHB Fifth Engineering Co., Ltd., respectively. Author Y.S., H.L., T.P., H.Z. and T.C. were employed by the company Zhuhai Communication Group. The remaining authors declare that the research was conducted in the absence of any commercial or financial relationships that could be construed as a potential conflict of interest.

References

1. Ghasali, E.; Orooji, Y.; Azarniya, A.; Alizadeh, M.; Kazem-zad, M.; Ebadzadeh, T. Production of V2C MXene using a repetitive pattern of V2AlC MAX phase through microwave heating of Al-V2O5-C system. *Appl. Surf. Sci.* **2021**, *542*, 148538. [[CrossRef](#)]
2. Zhang, F.; Yang, K.; Liu, G.; Chen, Y.; Wang, M.; Li, S.; Li, R. Recent advances on graphene: Synthesis, properties and applications. *Compos. Part A Appl. Sci. Manuf.* **2022**, *160*, 107051. [[CrossRef](#)]
3. Guo, F.; Li, L.; Shi, Y.; Shi, W.; Yang, X.; Li, H. Achieving superior anticorrosion and antibiofouling performance of polyani-line/graphitic carbon nitride composite coating. *Prog. Org. Coat.* **2023**, *179*, 107512. [[CrossRef](#)]
4. Shen, L.; Zhao, W.; Miao, L. Designed a novel EP plus GO/ZRC plus GO coating with bilayered structure for enhancing corrosion resistance of steel substrate. *J. Hazard. Mater.* **2021**, *403*, 123670. [[CrossRef](#)] [[PubMed](#)]
5. Xu, X.; Yi, D.; Wang, Z.; Yu, J.; Zhang, Z.; Qiao, R.; Sun, Z.; Hu, Z.; Gao, P.; Peng, H.; et al. Greatly Enhanced Anticorrosion of Cu by Commensurate Graphene Coating. *Adv. Mater.* **2018**, *30*, 1702944. [[CrossRef](#)] [[PubMed](#)]
6. Wang, X.; Zou, J.; Du, X.S. Facile flame catalytic growing carbon coating on Cu panel with surface protection performance comparable to that of graphene film via CVD. *Surf. Coat. Technol.* **2022**, *445*, 128720. [[CrossRef](#)]
7. Zou, J.; Wang, X.; Zhang, P.; Du, X. Ultrafast flame coating of carbon and chemical vapor deposition of graphene on NiTi alloy to enhance its corrosion resistance. *Diam. Relat. Mater.* **2022**, *128*, 109231. [[CrossRef](#)]
8. Cui, G.; Bi, Z.; Zhang, R.; Liu, J.; Yu, X.; Li, Z. A comprehensive review on graphene-based anti-corrosive coatings. *Chem. Eng. J.* **2019**, *373*, 104–121. [[CrossRef](#)]
9. Ding, R.; Zheng, Y.; Yu, H.; Li, W.; Wang, X.; Gui, T. Study of water permeation dynamics and anti-corrosion mechanism of graphene/zinc coatings. *J. Alloys Compd.* **2018**, *748*, 481–495. [[CrossRef](#)]
10. Halkjær, S.; Iversen, J.; Kyhl, L.; Chevallier, J.; Andreatta, F.; Yu, F.; Stoot, A.; Camilli, L.; Bøggild, P.; Hornekær, L. Low-temperature synthesis of a graphene-based, corrosion-inhibiting coating on an industrial grade alloy. *Corros. Sci.* **2019**, *152*, 1–9. [[CrossRef](#)]

11. Cheng, L.; Liu, C.; Han, D.; Ma, S.; Guo, W.; Cai, H.; Wang, X. Effect of graphene on corrosion resistance of waterborne inorganic zinc-rich coatings. *J. Alloys Compd.* **2019**, *774*, 255–264. [[CrossRef](#)]
12. Shen, L.; Li, Y.; Zhao, W.; Miao, L.; Xie, W.; Lu, H.; Wang, K. Corrosion Protection of Graphene-Modified Zinc-Rich Epoxy Coatings in Dilute NaCl Solution. *ACS Appl. Nano Mater.* **2019**, *2*, 180–190. [[CrossRef](#)]
13. Huang, S.; Kong, G.; Yang, B.; Zhang, S.; Che, C. Effects of graphene on the corrosion evolution of zinc particles in waterborne epoxy zinc-containing coatings. *Prog. Org. Coat.* **2020**, *140*, 105531. [[CrossRef](#)]
14. Cao, X.; Huang, F.; Huang, C.; Liu, J.; Cheng, Y.F. Preparation of graphene nanoplate added zinc-rich epoxy coatings for enhanced sacrificial anode-based corrosion protection. *Corros. Sci.* **2019**, *159*, 108120. [[CrossRef](#)]
15. Ding, R.; Li, W.; Wang, X.; Gui, T.; Li, B.; Han, P.; Tian, H.; Liu, A.; Wang, X.; Liu, X.; et al. A brief review of corrosion protective films and coatings based on graphene and graphene oxide. *J. Alloys Compd.* **2018**, *764*, 1039–1055. [[CrossRef](#)]
16. Ge, T.; Zhao, W.; Wu, X.; Lan, X.; Zhang, Y.; Qiang, Y.; He, Y. Incorporation of electroconductive carbon fibers to achieve enhanced anti-corrosion performance of zinc rich coatings. *J. Colloid Interface Sci.* **2020**, *567*, 113–125. [[CrossRef](#)]
17. Cho, S.; Chiu, T.M.; Castaneda, H. Electrical and electrochemical behavior of a zinc-rich epoxy coating system with carbon nanotubes as a diode-like material. *Electrochim. Acta* **2019**, *316*, 189–201. [[CrossRef](#)]
18. Zhou, S.; Wu, Y.; Zhao, W.; Yu, J.; Jiang, F.; Wu, Y.; Ma, L. Designing reduced graphene oxide/zinc rich epoxy composite coatings for improving the anticorrosion performance of carbon steel substrate. *Mater. Des.* **2019**, *169*, 107694. [[CrossRef](#)]
19. Dutta, G.K.; Karak, N. Bio-based waterborne polyester/cellulose nanofiber-reduced graphene oxide-zinc oxide nanocomposite: An approach towards sustainable mechanically robust anticorrosive coating. *Cellulose* **2022**, *29*, 1679–1703. [[CrossRef](#)]
20. Wu, Y.; Zhao, W.; Qiang, Y.; Chen, Z.; Wang, L.; Gao, X.; Fang, Z. π - π interaction between fluorinated reduced graphene oxide and acridizinium ionic liquid: Synthesis and anti-corrosion application. *Carbon* **2020**, *159*, 292–302. [[CrossRef](#)]
21. Cui, M.; Ren, S.; Zhao, H.; Xue, Q.; Wang, L. Polydopamine coated graphene oxide for anticorrosive reinforcement of water-borne epoxy coating. *Chem. Eng. J.* **2018**, *335*, 255–266. [[CrossRef](#)]
22. Li, Z.; Wang, X.; Zhang, Y.; Jing, C. Enhancing the Corrosion Resistance of Epoxy Coatings by Impregnation with a Reduced Graphene Oxide-Hydrophobic Ionic Liquid Composite. *ChemElectroChem* **2018**, *5*, 3300–3306. [[CrossRef](#)]
23. Parhizkar, N.; Shahrabi, T.; Ramezanzadeh, B. A new approach for enhancement of the corrosion protection properties and interfacial adhesion bonds between the epoxy coating and steel substrate through surface treatment by covalently modified amino functionalized graphene oxide film. *Corros. Sci.* **2017**, *123*, 55–75. [[CrossRef](#)]
24. Du, X.; Liu, H.Y.; Mai, Y.-W. Ultrafast Synthesis of Multifunctional NDoped Graphene Foam in an Ethanol Flame. *ACS Nano* **2016**, *10*, 453–462. [[CrossRef](#)] [[PubMed](#)]
25. Zhou, H.; Wang, H.; Du, X.; Zhang, Y.; Zhou, H.; Yuan, H.; Liu, H.-Y.; Mai, Y.-W. Facile fabrication of large 3D graphene filler modified epoxy composites with improved thermal conduction and tribological performance. *Carbon* **2018**, *139*, 1168–1177. [[CrossRef](#)]
26. Zhou, H.; Wang, H.; Du, X.; Mo, Y.; Yuan, H.; Liu, H.-Y. Hybrid three-dimensional graphene fillers and graphite platelets to improve the thermal conductivity and wear performance of epoxy composites. *Compos. Part A* **2019**, *123*, 270–277. [[CrossRef](#)]
27. Meng, W.; Du, X.; Ma, C.; Li, W. Highly Sensitive Flexible Poly(dimethylsiloxane) Composite Sensors Based on Flame-Synthesized Carbon Foam Made of Vertical Carbon Nanosheet Arrays. *ACS Sustain. Chem. Eng.* **2020**, *8*, 14091–14100. [[CrossRef](#)]
28. Meng, W.; Zou, J.; Wang, X.; Zhang, P.; Du, X. On the Distinctive Hardness, Anti-Corrosion Properties and Mechanisms of Flame-Deposited Carbon Coating with a Hierarchical Structure in Contrast to a Graphene Layer via Chemical Vapor Deposition. *Nanomaterials* **2022**, *12*, 2944. [[CrossRef](#)]
29. Ferrari, A.C.; Meyer, J.C.; Scardaci, V.; Casiraghi, C.; Lazzeri, M.; Mauri, F.; Piscanec, S.; Jiang, D.; Novoselov, K.S.; Roth, S.; et al. Raman spectrum of graphene and graphene layers. *Phys. Rev. Lett.* **2006**, *97*, 187401. [[CrossRef](#)]
30. Teng, S.; Gao, Y.; Cao, F.; Kong, D.; Zheng, X.; Ma, X.; Zhi, L. Zinc-reduced graphene oxide for enhanced corrosion protection of zinc-rich epoxy coatings. *Prog. Org. Coat.* **2018**, *123*, 185–189. [[CrossRef](#)]
31. Ramezanzadeh, B.; Mohamadzadeh Moghadam, M.H.; Shohani, N.; Mahdavian, M. Effects of highly crystalline and conductive polyaniline/graphene oxide composites on the corrosion protection performance of a zinc-rich epoxy coating. *Chem. Eng. J.* **2017**, *320*, 363–375. [[CrossRef](#)]
32. Mo, M.; Zhao, W.; Chen, Z.; Yu, Q.; Zeng, Z.; Wu, X.; Xue, Q. Excellent tribological and anti-corrosion performance of polyurethane composite coatings reinforced with functionalized graphene and graphene oxide nanosheets. *RSC Adv.* **2015**, *5*, 56486–56497. [[CrossRef](#)]
33. Yun, T.H.; Park, J.H.; Kim, J.S.; Park, J.M. Effect of the surface modification of zinc powders with organosilanes on the corrosion resistance of a zinc pigmented organic coating. *Prog. Org. Coat.* **2014**, *77*, 1780–1788. [[CrossRef](#)]
34. Mouanga, M.; Berçot, P.; Rauch, J.Y. Comparison of corrosion behaviour of zinc in NaCl and in NaOH solutions. Part I: Corrosion layer characterization. *Corros. Sci.* **2010**, *52*, 3984–3992. [[CrossRef](#)]
35. De la Fuente, D.; Castaño, J.G.; Morcillo, M. Long-term atmospheric corrosion of zinc. *Corros. Sci.* **2007**, *49*, 1420–1436. [[CrossRef](#)]

36. Li, X.; Cubides, Y.; He, Z.; Soucek, M.D.; Castaneda, H. Corrosion Assessment of Zinc-Rich Primers Containing Polyaniline and the Effect of Acid as a Dopant. *Corrosion* **2018**, *74*, 1141–1157. [[CrossRef](#)]
37. Xie, D.-M.; Huang, K.; Feng, X.; Wang, Y.-G. Improving the performance of zinc-rich coatings using conductive pigments and silane, Corrosion Engineering. *Sci. Technol.* **2020**, *55*, 539–549.

Disclaimer/Publisher's Note: The statements, opinions and data contained in all publications are solely those of the individual author(s) and contributor(s) and not of MDPI and/or the editor(s). MDPI and/or the editor(s) disclaim responsibility for any injury to people or property resulting from any ideas, methods, instructions or products referred to in the content.